Appl. Phys. B 67, 5–10 (1998)

Applied Physics B
Lasers
and Optics

1.24-μm cascaded Raman laser for 1.31-μm Raman fiber amplifiers

A. Bertoni[1,*], **G.C. Reali**[2]

[1] INFM - Dep. of Nuclear and Theoretical Physics, University of Pavia, via Bassi, 6 - 27100 Pavia, Italy
(Fax: +39-382/526938, E-mail: bertoni@pavia.infn.it)
[2] INFM - Dep. of Electronics, University of Pavia, via Ferrata, 1 - 27100 Pavia, Italy
(Fax: +39-382/422583, E-mail: realilab@dragon.ian.pv.cnr.it)

Received: 10 November 1997

Abstract. A novel set of normalized coupled nonlinear differential equations drawn after Von der Linde et al. is used to describe stimulated Raman scattering in optical fibers. The numerical solutions of the differential system lead in a natural way to the calculation of the ratio between Stokes and pump powers at the output end of the fiber. The model is exploited to deduce the optimum performances of a 1.064-μm pumped third-order cascaded Raman laser operating at the wavelength of 1.24 μm in cw regime of operation, whose output should be useful in pumping a 1.31-μm fiber amplifier.

PACS: 42.60D; 42.80

Since the majority of terrestrial optical communication systems currently operate at wavelengths close to 1.3 μm, there is a need for amplifiers that regenerate the signals travelling at this wavelength. Very few proposals have been advanced, without success, and it appears that even the recently proposed amplifiers based on Pr^{+3}-doped fluoride fibers (PDFAs) [1, 2] suffer a number of disadvantages. A technique proposed earlier, based on stimulated Raman scattering (SRS), has been re-examined and found to be still a robust candidate for amplification of the signal transmitted at 1.31 μm.

Raman amplification of the signal at 1.31 μm requires the availability of a pump source at 1.24 μm. Fiber laser emission at this wavelength can be obtained through a third-order Raman cascade pumped by a Nd^{+3}-doped double-clad fiber laser output at 1.064 μm [3–5] in high-delta-GeO_2-doped silica fibers, where feedback is provided by low-loss, high-reflectivity fiber Bragg gratings (FBGs) [6].

A number of papers employing this scheme have recently been presented [7–9] and shows that SRS indeed offers a rugged and reliable alternative to PDFAs. A novel theoretical model is presented for the analysis of fiber laser performances in the following.

The numerical solution of this model allows us to calculate the ratio between Stokes output powers and fiber-coupled pump powers under the assumption of fiber single-mode operation at the wavelengths of the beams involved in SRS.

In Sect. 1 a description of the theoretical model employed in the calculation of Stokes modes output powers is reported. It is an extension to fiber resonators of a model first introduced by Von der Linde et al. [10, 11] for the description of Raman amplification of light pulses in CS_2. In Sect. 2 a comparison is made between the results of the simulation of fiber laser performances obtained using this model and those obtained by a previously described model which relies on a set of coupled nonlinear differential equations in terms of beam effective powers [12]. In Sect. 3 our conclusions are finally presented.

1 Theoretical model

In a preceding paper [12] the single-pass evolution of pump and higher order Stokes beams of the Raman laser has been described in terms of effective powers that take into account the finite width intensity distributions of the beams involved in SRS through the calculation of the beam power fraction in the fiber core. The definition of effective powers relies on the introduction of effective core areas which appear explicitly in the set of the nonlinearly coupled equations which describe SRS within that model.

Another way to take care of the finite beam width is to start directly from the set of nonlinearly coupled equations for beam intensities [13]:

$$\begin{aligned}
\frac{\mathrm{d}I_\mathrm{p}}{\mathrm{d}z} &= -g_\mathrm{R}\frac{\nu_\mathrm{p}}{\nu_{\mathrm{s}_1}} I_\mathrm{p} I_{\mathrm{s}_1} - \alpha_\mathrm{p} I_\mathrm{p} \\
\frac{\mathrm{d}I_{\mathrm{s}_1}}{\mathrm{d}z} &= g_\mathrm{R} I_\mathrm{p} I_{\mathrm{s}_1} - g_\mathrm{R}\frac{\nu_{\mathrm{s}_1}}{\nu_{\mathrm{s}_2}} I_{\mathrm{s}_1} I_{\mathrm{s}_2} - \alpha_{\mathrm{s}_1} I_{\mathrm{s}_1} \\
\frac{\mathrm{d}I_{\mathrm{s}_2}}{\mathrm{d}z} &= g_\mathrm{R} I_{\mathrm{s}_1} I_{\mathrm{s}_2} - g_\mathrm{R}\frac{\nu_{\mathrm{s}_2}}{\nu_{\mathrm{s}_3}} I_{\mathrm{s}_2} I_{\mathrm{s}_3} - \alpha_{\mathrm{s}_2} I_{\mathrm{s}_2} \\
\frac{\mathrm{d}I_{\mathrm{s}_3}}{\mathrm{d}z} &= g_\mathrm{R} I_{\mathrm{s}_2} I_{\mathrm{s}_3} - g_\mathrm{R}\frac{\nu_{\mathrm{s}_3}}{\nu_{\mathrm{s}_4}} I_{\mathrm{s}_3} I_{\mathrm{s}_4} - \alpha_{\mathrm{s}_3} I_{\mathrm{s}_3} \\
\frac{\mathrm{d}I_{\mathrm{s}_4}}{\mathrm{d}z} &= g_\mathrm{R} I_{\mathrm{s}_3} I_{\mathrm{s}_4} - \alpha_{\mathrm{s}_4} I_{\mathrm{s}_4}\,, \qquad (1)
\end{aligned}$$

* Corresponding author

where I_i, ν_i, α_i, $i = \mathrm{p}, \mathrm{s}_1, \ldots, \mathrm{s}_4$ represent the beam intensities, the frequencies, and the attenuations at pump and higher order Stokes modes wavelengths, respectively.

We now introduce the following adimensional parameters:

$$\begin{aligned} Z &= z g_\mathrm{R} I_\mathrm{p}(0,r) \\ \beta_i &= \alpha_i / g_\mathrm{R} I_\mathrm{p}(0,r), \quad i = \mathrm{p}, \mathrm{s}_1, \ldots, \mathrm{s}_4 , \end{aligned} \tag{2}$$

where z is the longitudinal coordinate of propagation along the fiber axis, $I_\mathrm{p}(0,r)$ is the pump intensity distribution at $z = 0$ and g_R is the Raman gain coefficient at the pump wavelength. The initial pump intensity distribution is regarded as a function of the radial coordinate in a plane normal to the beam direction of propagation as a consequence of the assumption of laser single-mode operation. The beam intensities are then replaced by the following normalized intensity functions:

$$K_i(Z) = I_i(Z)/I_\mathrm{p}(0,r) \quad i = \mathrm{p}, \mathrm{s}_1, \ldots, \mathrm{s}_4 \tag{3}$$

which allow us to put the differential system (1) in the following form:

$$\begin{aligned} \frac{\mathrm{d}K_\mathrm{p}}{\mathrm{d}Z} &= -\frac{\nu_\mathrm{p}}{\nu_{\mathrm{s}_1}} K_\mathrm{p} K_{\mathrm{s}_1} - \beta_\mathrm{p} K_\mathrm{p} \\ \frac{\mathrm{d}K_{\mathrm{s}_1}}{\mathrm{d}Z} &= K_\mathrm{p} K_{\mathrm{s}_1} - \frac{\nu_{\mathrm{s}_1}}{\nu_{\mathrm{s}_2}} K_{\mathrm{s}_1} K_{\mathrm{s}_2} - \beta_{\mathrm{s}_1} K_{\mathrm{s}_1} \\ \frac{\mathrm{d}K_{\mathrm{s}_2}}{\mathrm{d}Z} &= K_{\mathrm{s}_1} K_{\mathrm{s}_2} - \frac{\nu_{\mathrm{s}_2}}{\nu_{\mathrm{s}_3}} K_{\mathrm{s}_2} K_{\mathrm{s}_3} - \beta_{\mathrm{s}_2} K_{\mathrm{s}_2} \\ \frac{\mathrm{d}K_{\mathrm{s}_3}}{\mathrm{d}Z} &= K_{\mathrm{s}_2} K_{\mathrm{s}_3} - \frac{\nu_{\mathrm{s}_3}}{\nu_{\mathrm{s}_4}} K_{\mathrm{s}_3} K_{\mathrm{s}_4} - \beta_{\mathrm{s}_3} K_{\mathrm{s}_3} \\ \frac{\mathrm{d}K_{\mathrm{s}_4}}{\mathrm{d}Z} &= K_{\mathrm{s}_3} K_{\mathrm{s}_4} - \beta_{\mathrm{s}_4} K_{\mathrm{s}_4} \end{aligned} \tag{4}$$

Both the adimensional parameter Z and the normalized attenuation coefficients β_i, $i = \mathrm{p}, \mathrm{s}_1, \ldots, \mathrm{s}_4$ depend on the pump intensity distribution at $z = 0$.

It is possible to solve the differential system (4) distinguishing the two following cases:

1. the normalized intensities K are calculated for a given value of incident pump intensity as a function of the distance of propagation along the fiber axis;
2. the normalized intensity functions are calculated for a given fiber length as a function of incident pump intensity.

Since our scope is to analyse the effect of a definite beam intensity distribution over the fiber cross section we chose to deal with the second case. In what follows the numerical integration of the differential set of nonlinearly coupled equations (4) will be given assuming a fixed fiber length as a function of the initial pump intensity values. If the fiber length is fixed, the differential system can be set in a more practical form by an appropriate change of representation. We define a new set of functions K' given by:

$$K'_i = K_i \exp(\beta_i Z) . \tag{5}$$

In terms of the K' functions the set of differential equations assumes the following form:

$$\begin{aligned} \frac{\mathrm{d}K'_\mathrm{p}}{\mathrm{d}Z} &= -\frac{\nu_\mathrm{p}}{\nu_{\mathrm{s}_1}} K'_\mathrm{p} K'_{\mathrm{s}_1} \exp(-\alpha_{\mathrm{s}_1} L) \\ \frac{\mathrm{d}K'_{\mathrm{s}_1}}{\mathrm{d}Z} &= K'_\mathrm{p} K'_{\mathrm{s}_1} \exp(-\alpha_\mathrm{p} L) - \frac{\nu_{\mathrm{s}_1}}{\nu_{\mathrm{s}_2}} K'_{\mathrm{s}_1} K'_{\mathrm{s}_2} \exp(-\alpha_{\mathrm{s}_2} L) \\ \frac{\mathrm{d}K'_{\mathrm{s}_2}}{\mathrm{d}Z} &= K'_{\mathrm{s}_1} K'_{\mathrm{s}_2} \exp(-\alpha_{\mathrm{s}_1} L) - \frac{\nu_{\mathrm{s}_2}}{\nu_{\mathrm{s}_3}} K'_{\mathrm{s}_2} K'_{\mathrm{s}_3} \exp(-\alpha_{\mathrm{s}_3} L) \\ \frac{\mathrm{d}K'_{\mathrm{s}_3}}{\mathrm{d}Z} &= K'_{\mathrm{s}_2} K'_{\mathrm{s}_3} \exp(-\alpha_{\mathrm{s}_2} L) - \frac{\nu_{\mathrm{s}_3}}{\nu_{\mathrm{s}_4}} K'_{\mathrm{s}_3} K'_{\mathrm{s}_4} \exp(-\alpha_{\mathrm{s}_4} L) \\ \frac{\mathrm{d}K'_{\mathrm{s}_4}}{\mathrm{d}Z} &= K'_{\mathrm{s}_3} K'_{\mathrm{s}_4} \exp(-\alpha_{\mathrm{s}_3} L) . \end{aligned} \tag{6}$$

The gain and loss coefficients for the K' functions are determined both by the attenuation coefficients and by the fixed fiber length L.

The main parameters we are interested in are the ratios between Stokes beams output powers and fiber-coupled pump power:

$$\mathfrak{R}_\mathrm{i} = \frac{P_\mathrm{j}(L)}{P_\mathrm{p}(0)} \tag{7}$$

The pump intensity distribution on the fundamental mode can be approximated by a Gaussian function,

$$I_\mathrm{p}(0,r) = I_\mathrm{p}(0,0) \exp(-2(r/w_\mathrm{p})^2) , \tag{8}$$

where w_p is fundamental modal beam radius [14], and the power ratios at the output end of the fiber can then be calculated as:

$$\mathfrak{R}_\mathrm{j} = \frac{\int_0^\infty I_\mathrm{p}(0,r) K_\mathrm{j}(I_\mathrm{p}(0,r)) r \,\mathrm{d}r}{\int_0^\infty I_\mathrm{p}(0,r) r \,\mathrm{d}r} . \tag{9}$$

By changing the variable of integration, the power ratios can be written as follows:

$$\mathfrak{R}_\mathrm{j} = \frac{\int_0^{I_\mathrm{p}(0,0)} K_\mathrm{j}(I) \,\mathrm{d}I}{I_\mathrm{p}(0,0)} , \tag{10}$$

where $I_\mathrm{p}(0,0)$ is the pump peak intensity at $z = 0$. A further change of the variable of integration allows the power ratios to be directly evaluated in terms of the adimensional parameter Z.

$$\mathfrak{R}_\mathrm{j} = \frac{P_\mathrm{j}(L)}{P_\mathrm{p}(0)} = \frac{\int_0^{Z_\mathrm{f}} K_\mathrm{j}(Z) \,\mathrm{d}Z}{Z_\mathrm{f}} , \tag{11}$$

where the upper extreme of integration is given by:

$$Z_\mathrm{f} = z g_\mathrm{R} I_\mathrm{p}(0,0) . \tag{12}$$

The normalized intensity functions $K(Z)$ which are requested for the calculation of the power ratios can be obtained by integrating the differential system (6) between 0 and Z_f and inverting (5).

The initial conditions for the normalized intensity functions in the new representation have been approximated as follows:

$$K'_{\mathrm{p}} = 1 \quad K'_{\mathrm{s_i}} = \frac{P_{\mathrm{noise}}}{P_{\mathrm{p}}^{\mathrm{eff}}(0)} \tag{13}$$

where P_{noise} is the spontaneous emission contribution to Stokes mode power [12] and $P_{\mathrm{p}}^{\mathrm{eff}}(0)$ represents the effective fiber-coupled pump power. The numerical integration of the differential system, subjected to appropriate boundary conditions for each Stokes component, has been performed using either a standard Runge–Kutta numerical integration method or a stiff integrator, giving results in substantial agreement in both cases. In Fig. 1 the nomalized intensity functions K are plotted vs $I_{\mathrm{p}}(0, r)$ for a 800-m-long fiber sample with a 26% GeO_2 dopant concentration (ϱ) in the fiber core, a maximum index difference Δ of 0.036 and a cutoff wavelength of 0.98 μm. The value of Raman gain coefficient has been deduced from [15], taking into account the inverse dependence on pump wavelength [16], the linear dependence on GeO_2 dopant concentration [17] and the fact that the Raman gain coefficient for GeO_2 fibers is about eight times higher than for SiO_2 fibers [18]. Note that the value reported in [15] is about half the value reported in [19] in order to account for the effects of polarization scrambling. By making use of (11) the Stokes-to-pump power ratios have been obtained as a function of pump peak intensities (Fig. 2).

If we compare the results reported in Fig. 1 with those in Fig. 2 we observe that power ratios rise to a maximum value within the range of pump intensities where the K_i functions have substantial values and for laser intensities beyond this range they are inversely proportional to $I_{\mathrm{p}}(0, 0)$.

The results reported in Fig. 2 differ from those obtained by integrating the nonlinear differential system for the effective powers [12] in that the pump and the Stokes modes powers show up simultaneously at the fiber end. In the former case only one Stokes beam, or at most two of them, are present at the end of the fiber, all the others being vanishingly small.

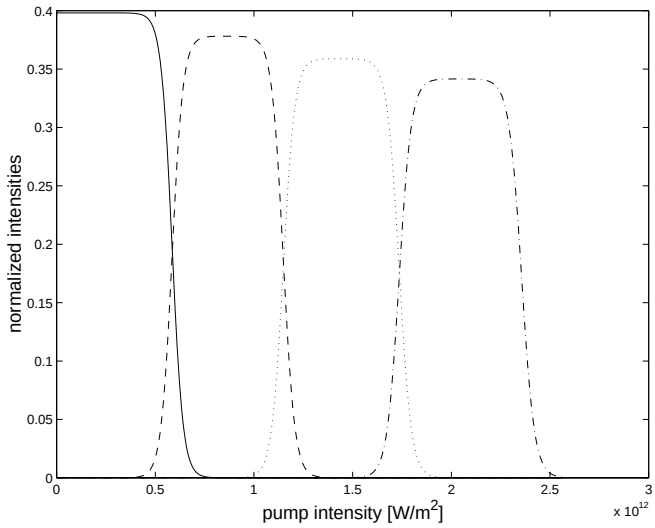

Fig. 1. Normalized intensities vs pump intensities at $z = 0$, $\mathrm{I_p}(0, r)$ for a 800-m 26% GeO_2-doped fiber sample with a 0.98-μm cutoff wavelength and 0.036 maximum index difference

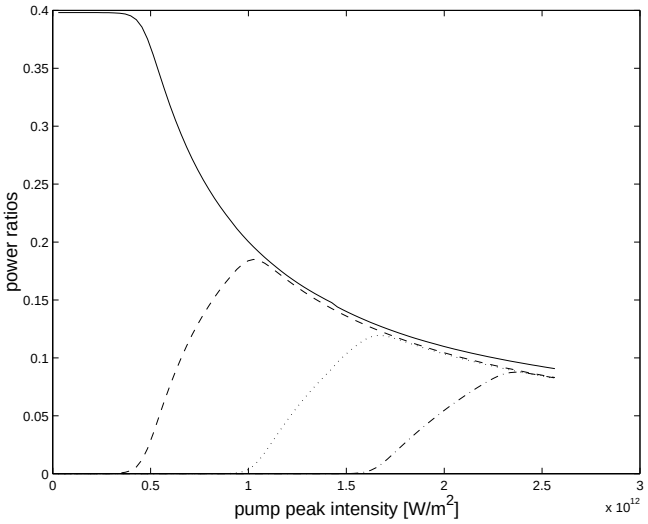

Fig. 2. Power ratios $\Re$ at the output end of a 800-m 26% GeO_2-doped fiber sample with a 0.98-μm cutoff wavelength and 0.036 maximum index difference as a function of pump peak intensity at $z = 0$

For the simulation of beam propagation of the cascaded fiber Raman laser, the initial conditions for the beam successive passages in the resonator cavity have been determined by averaging the normalized intensity functions K obtained from the numerical integration over the previous passage between 0 and Z_{f}. As it is evident from (7) Z_{f} is a function of the pump peak intensity value.

In the forward propagation passages the pump peak intensity value is fixed for a given input pump power whereas in the backward direction it has to be determined from effective residual pump power after reflection off the cavity output mirrors.

2 Results of the simulations

The calculated values of slope efficiencies, maximum conversion efficiencies, thresholds, and figures of merit obtained within the model described above have been plotted against fiber cavity length for two fiber samples with different dopant concentrations. The plots are reported in Figs. 3 and 4 for two different values of the third Stokes output coupling coefficient, the relevant fiber parameters being specified in each figure caption.

The figure of merit has been defined as the ratio between slope efficiencies and threshold powers corresponding to a given fiber length:

$$\Re = \frac{\text{slope efficiency}}{P_{\mathrm{th}}}\,. \tag{14}$$

The slope efficiency behaviour as a function of fiber length is determined by the cavity losses: as a matter of fact slope efficiencies are lower for 20% output coupling configurations and, for a given value of third Stokes output coupling, for the most strongly doped fiber sample which is also characterized by a faster decrease of slope efficiency with fiber lengths. The

threshold decrease with fiber lengths is exponential: thresholds are lower for the most strongly doped fiber sample which features both higher Raman gain coefficient and smaller core areas. For both values of third Stokes output couplings the optimum resonator performance is obtained using the most strongly doped fiber sample.

For a 20% third Stokes output coupling, the optimum resonator performance (determined by the maximum value of the figure of merit) corresponds to a fiber length of 400 m of the most strongly doped fiber sample. This cavity configuration features a threshold of 153 mW and a slope efficiency of 51%. For a 4% output coupling, the optimum resonator

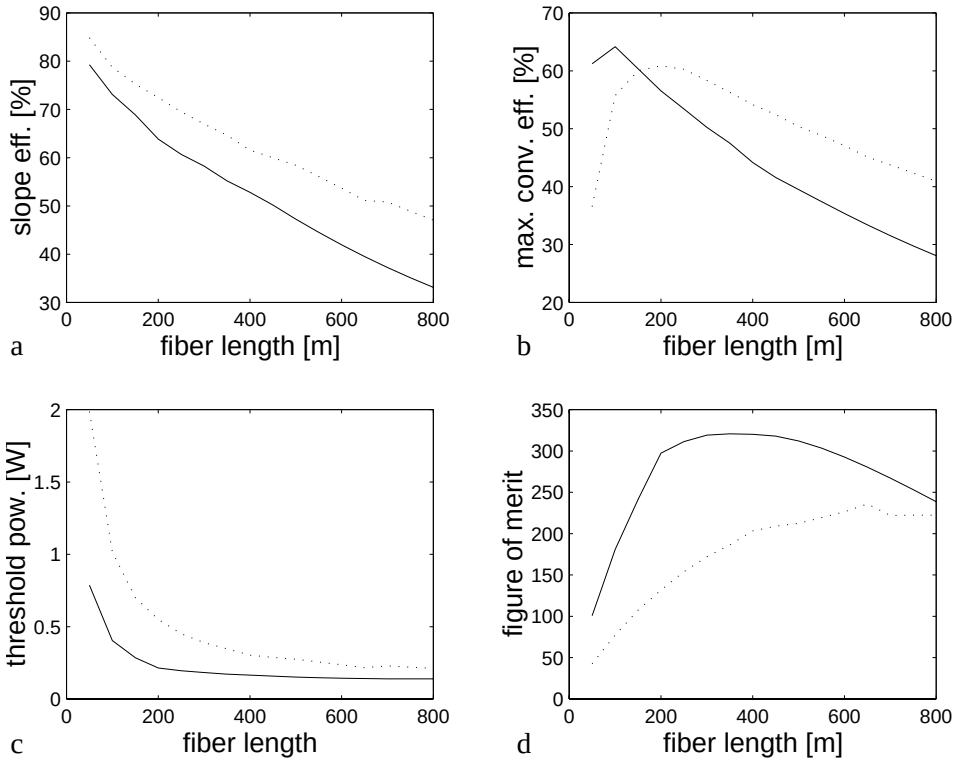

Fig. 3a–d. Comparison between the calculated values of: **a** slope efficiencies, **b** maximum conversion efficiencies, **c** thresholds, **d** figure of merit vs fiber length for a third-order cascaded Raman resonator with 20% third Stokes output coupler for two fiber samples with different dopant concentration. Fiber parameters: $\varrho = 18\%$, $\Delta = 0.026$, $\lambda_c = 1\,\mu\text{m}$ (*dotted line*); $\rho = 26\%$, $\Delta = 0.036$, $\lambda_c = 0.98\,\mu\text{m}$ (*solid line*)

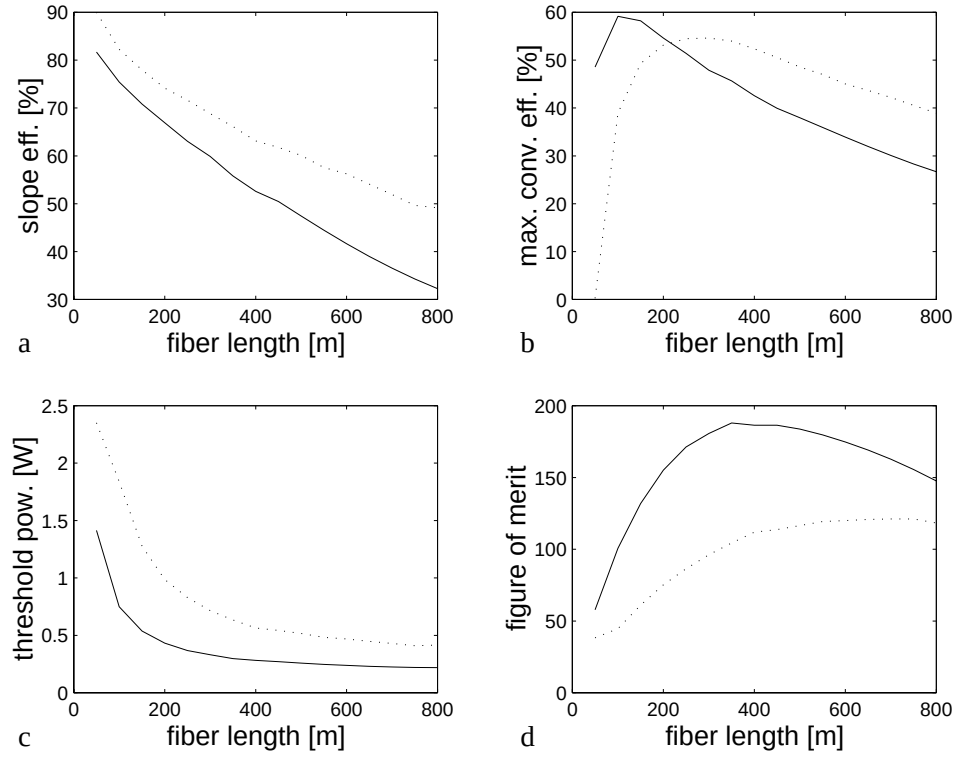

Fig. 4a–d. Comparison between the calculated values of: **a** slope efficiencies, **b** maximum conversion efficiencies, **c** thresholds, **d** figure of merit vs fiber length for a third-order cascaded Raman resonator with 4% third Stokes output coupler for two fiber samples with different dopant concentration. Fiber parameters: $\rho = 18\%$, $\Delta = 0.026$, $\lambda_c = 1\,\mu\text{m}$ (*dotted line*); $\rho = 26\%$, $\Delta = 0.036$, $\lambda_c = 0.98\,\mu\text{m}$ (*solid line*)

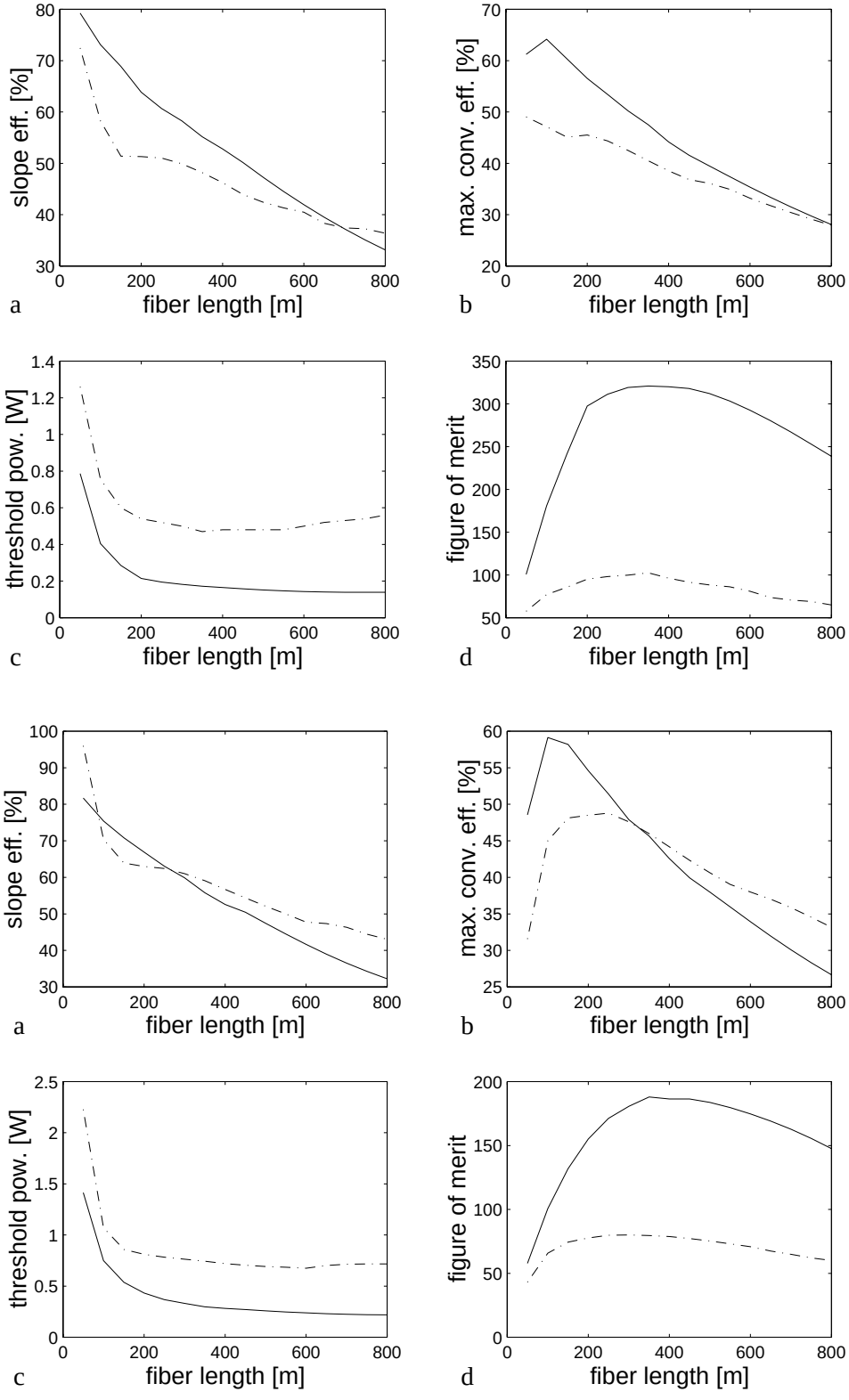

Fig. 5a–d. Comparison between the calculated values of: **a** slope efficiencies, **b** maximum conversion efficiencies, **c** thresholds, **d** figure of merit vs fiber length for a third-order cascaded Raman resonator with 4% third Stokes output coupling within model I (*dashed-dotted line*) and model II (*solid line*). Fiber parameters: $\rho = 18\%$, $\Delta = 0.026$, $\lambda_c = 1\,\mu\text{m}$

Fig. 6a–d. Comparison between the calculated values of: **a** slope efficiencies, **b** maximum conversion efficiencies, **c** thresholds, **d** figure of merit vs fiber length for a third-order cascaded Ramam resonator with 20% third Stokes output coupling within model I (*dashed-dotted line*) and model II (*solid line*). Fiber parameters: $\rho = 18\%$, $\Delta = 0.026$, $\lambda_c = 1\,\mu\text{m}$

performance corresponds to a fiber length of 400 m of the most strongly doped fiber sample. This cavity configuration features a threshold of 260 mW and a slope efficiency of 51.1%. The calculated values of the parameters defining the fiber laser performance for a 20% output coupling are in good agreement with the performance parameters obtained by Grubb and co-workers using a 800-m-high delta-GeO_2-doped fiber and a 20% third Stokes output coupler [7] whereas for a 4% output coupling the calculated value of threshold is almost halved and slope efficiency is slightly lower [7]. In Figs. 5 and 6 the performance parameters calculated with the model described in the present work (model II) are compared

with those obtained within the previously reported model (model I) for the most strongly doped fiber sample. As shown in the figures the main differences between the two sets of calculated values are as follows.

1. The slope efficiencies obtained within model II show a roughly linear decrease with fiber lengths within the range of fiber lengths taken into consideration in the simulations whereas those calculated within model I feature a rapid decrease with fiber lengths for small fiber lengths and a slower decrease for longer fiber lengths;
2. The calculated thesholds within model II are considerably lower than those of model I;
3. The maximum conversion efficiencies calculated within model II reach higher values than those calculated within model I but show a faster decrease with fiber length for long fiber lengths.

The apparent contradiction between these results is a consequence of the fact that our model predicts third Stokes linear power scaling within the range of input pump powers taken into consideration (up to 3.5 W) only for relatively small fiber lengths. By increasing the fiber cavity length the range of input pump powers over which the resonator features linear power scaling narrows. In fact, by increasing the fiber cavity length, the fourth Stokes Raman thresholds decrease resulting in a rapid depletion of the third Stokes beam. This fact may be regarded as a consequence of the use of fibers with both high dopant concentration and extremely small core areas (the fiber core diameters being less than 3 μm for the most strongly doped fiber sample).

3 Conclusion

A redefined model for the description of a third-order cascaded Raman laser operation has been reported where the finite width beam transverse modal distribution has been taken into account. The set of normalized nonlinearly coupled differential equations describing SRS has been integrated for a number of fibers of different lengths corresponding to different laser cavities.

The results have been compared with those obtained within a prevously reported model where the beam propagation has been described in terms of effective powers. The main differences between the two sets of calculated values arise from the presence of lower threshold powers, slope efficiencies, and maximum conversion efficiencies.

The lower values of maximum conversion efficiencies are a consequence of the fact that our model predicts linear power scaling of third Stokes output power only within a limited range of input pump powers; the decrease of third Stokes maximum conversion efficiencies with fiber length is faster for the most strongly doped fiber sample. The results of the simulations show that maximum conversion efficiencies of fiber-coupled pump power up to 60% are reachable both for a 26% GeO_2-doped fiber sample both for 20% and 4% third Stokes output couplings. The values calculated within this model are in good agreement with the reported experimental values of slope efficiencies and thresholds for 20% output coupling: for a 4% third Stokes output coupling the calculated threshold value is even much lower than the reported experimental value (it is almost halved).

It is our opinion that this model provides a more realistic description of the performance of a cascaded fiber Raman laser than the previously reported model since it relies on a differential system where the functions to be integrated are the conversion efficiencies of the pump intensity components across the fiber section, thus being more sensitive to the effective spatial intensity distribution than a model where the beams are approximated by plane waves with constant intensities across planes normal to the beam direction of propagation.

Acknowledgements. The authors wish to thank the Istituto di Analisi Numerica of CNR, Pavia for the computer facilities, both hardware and software.

References

1. E. Ishikawa, H. Yanagita, K. Itoh, H. Aoki, H. Toratani: OAA '96 Monterey CA, paper ThC2-1 (1996)
2. J. Kobelke, M. Duhamel, F. Chatton, T. Georges: OAA '96 Monterey CA, paper FD1-1 (1996)
3. H. Po, J.D. Cao, B.M. Laliberte, R.A. Minns, R.F. Robinson, B.H. Rockney, R.R. Tricca, Y.H. Zhang: Electron. Lett. **29**, 1500 (1993)
4. H. Zellmer, U. Willamowsky, A. Tunnermann, H. Welling, S. Unger, V. Reichel, H.R. Muller, J. Kirchhof, P. Albers: Opt. Lett. **20**, 578 (1995)
5. D. Inissis, D.J. DiGiovanni, T.A. Strasser, A. Hale, C. Headley, A.J. Stentz, R. Pedrazzani, D. Tipton, S.G. Kosinsky, D.L. Brownlow, K.W. Quoi, K.S. Kranz, R.G. Huff, R. Espindola, J.D. LeGrange, G. Jacobovitz-Veselka, D. Boggavarapu, X. He, D. Caffey, S. Gupta, S. Srinivasan, K. McEuen, R. Patel: CLEO '97 Post-deadline papers, CPD31-1 (1997)
6. G. Meltz, W.W. Morey, W.H. Glen: Opt. Lett. **14**, 823 (1989)
7. S.G. Grubb: Proc. OSA OAA '95 Davos, SaA1-1 (1995)
8. E. Dianov, D.G. Fursa, A.A. Abramov, M.M. Bubnov, A.M. Prukhorov, A.V. Shipulin, G.G. Devjatykh, A.G. Guryanov, V.F. Khopin: Electron. Lett. **31**, 1057 (1995)
9. P.B. Hansen, A.J. Stentz, L. Eskildsen, S.G. Grubb, T.A. Strasser, J.R. Pedrazzani: Proc. OAA '96 Monterey, PDP1-1 (1996)
10. D. Von der Linde, M. Maier, W. Kaiser: Phys. Rev. **178**, 11 (1969)
11. W. Kaiser, M. Maier: *Laser Handbook*, 2nd edn., ed. by F.T. Arecci (North Holland, Amsterdam 1972) pp. 1077–1150
12. A. Bertoni: Opt. Quantum Electron. **29**, 1047 (1997)
13. Y.R. Shen, N. Bloembergen: Phys. Rev. **137A**, 1767 (1965)
14. D. Marcuse: J. Opt. Soc. Am. **68**, 103 (1978)
15. D. Mahgerefteh, D.L. Butler, J. Goldhar, L.G. Joneckis: OFC'97 Tech. Dig., p. 188 (1997)
16. G.P. Agrawal: *Non linear fiber optics*, 2nd. edn. (Academic Press, San Diego 1995) p. 318
17. S.T. Davey, D.L. Williams, B.J. Ainslie, W.J.M. Rothwell, B. Wakefield: IEE Proc. **136**, 301 (1989)
18. F.L. Galeener, J.C. Mikkelsen, R.H. Geils, W.J. Mosby: Appl. Phys. Lett. **32**, 34 (1978)
19. R.H. Stolen, E.P. Ippen: Appl. Phys. Lett. **22**, 276 (1978)